Journal of Statistical Physics, Vol. 45, Nos. 5/6, 1986

Magnetic Phase Structure on the Penrose Lattice

C. Godrèche,[1] J. M. Luck,[2] and H. Orland[2]

Received July 10, 1986

The Ising model on a two-dimensional Penrose tiling is studied by means of the Migdal–Kadanoff scheme. This approximate renormalization method closely follows the inflation rules of the tiling, which are easily described in terms of Robinson triangles, and lead to the consideration of four types of nearest neighbor couplings. The ferromagnetic phase transition is similar to the usual one encountered on periodic lattices. When the couplings have both signs, the presence of frustration without randomness yields a fairly intricate phase diagram, essentially made up of two regions with a very complicated border. Region I consists of "quasiferromagnetic" models, which exhibit long-range order below some finite critical temperature. The models of region II are paramagnetic at nonzero (low) temperature, but may become ordered (reentrant phases) in a higher temperature range.

KEY WORDS: Quasicrystals; real-space renormalization; Ising model; frustration; phase transitions; reentrant phases.

1. INTRODUCTION

The discovery of quasicrystals[1] started an intense theoretical activity.[2] Much of this activity is devoted to the study of the structure and cristallography of these new phases. Other studies concern their stability, elementary excitations, etc. In this paper we investigate the magnetic properties of quasicrystals.

Quasilattices are the realization of quasiperiodic objects in two or three dimensions. In the same way as the well-known one-dimensional incommensurate structures have at least two periods in competition, the Penrose lattice,[3] for instance, is described by five incommensurate periods.

[1] Service de Physique du Solide et de Résonance Magnétique, CEN-Saclay, 91191 Gif-sur-Yvette Cedex, France.
[2] Service de Physique Théorique, CEN-Saclay, 91191 Gif-sur-Yvette Cedex, France.

0022-4715/86/1200-0777$05.00/0

This is clearly shown by the projection method.[4-7] Hence, those structures are intermediate between periodic systems and random ones, and, generalizing the case of incommensurate structures, they are geometrically frustrated objects.

Another kind of frustration is met in magnetic systems.[8] Frustration is responsible for unusual properties in random magnetic models, such as spin glasses. Its effects have also been studied in the case of hierarchical nonrandom systems.[9,10] It is thus tempting, apart from the direct physical interest of the problem, to study the effects of frustration without disorder on a quasiperiodic system.

Let us consider the Ising model on a 2D Penrose tiling. This tiling is a generic example of a quasicrystal. The Hamiltonian of the system reads

$$\mathscr{H} = -\sum_{\langle i,j \rangle} J_{ij} S_i S_j \tag{1.1}$$

where $\langle i, j \rangle$ are nearest neighbors, and $S_i = \pm 1$ are spins located on the vertices of the tiling. The magnetic interactions between the atoms are described by coupling constants J_{ij}. Their values are given by geometrical rules described below. Since the locations of points of the lattice are quasiperiodic, the connectivities and coupling constants are quasiperiodic, too.

The aim of the present paper is to study the properties (phase diagram, critical temperatures, etc.) of this model. Since an analytical approach seems very difficult (it is already the case for simpler linear problems, such as phonon spectra) we choose to use an appropriate kind of real-space renormalization group method.

In Section 2, we describe the model and its basic properties. We consider here the Penrose tiling obtained with Robinson triangles.[11,12] These tiles are well fitted to describe simply the inflation/deflation (or decomposition/composition) properties of the tiling. We will indeed rely heavily upon these geometrical self-similarity properties in order to define in a natural and minimal way the coupling constants J_{ij} and to renormalize the system. The Migdal–Kadanoff[13,14] scheme is the natural method to use in our case, since it follows exactly the geometry of the tiling. In particular, the renormalization is done in two steps, using two types of blocks.

In Section 3 we study the physical properties of the model (ferromagnetic transition, phase diagram at zero and finite temperature). The Migdal–Kadanoff method leads to a mapping in four variables, which exhibits a rich variety of phases. In the frustrated region (when some of the couplings are negative), infinitely many ordered (quasiferromagnetic) phases are present, with possible reentrant behavior. The ferromagnetic transition, and in particular its critical behavior, is expected to be similar

to that encountered in a regular lattice. Indeed, critical properties of the two-dimensional Ising model are determined by the low-frequency behavior of the Laplacian operator on the lattice, which should be *a priori* fairly similar to the periodic case.

This work is a continuation of previous studies by the authors: in Ref. 15 a one-dimensional Ising model in a quasiperiodic magnetic field was studied. It exhibits an infinity of modulated phases at zero temperature (see also Refs. 16 and 17). In Ref. 18 the same geometrical properties as in the present paper were used, but another approximate renormalization scheme, namely the cumulant method,[19] was chosen, and spins were put on the dual lattice. The intricacy of the eight-dimensional mapping that emerges from that method led us to the present work.

2. THE MODEL: RENORMALIZATION AND BASIC PROPERTIES

2.1. Penrose Tiling with Robinson Triangles

The *Penrose tiling* mentioned in the introduction is usually described as being made of darts and kites, or of two species of rhombs. The latter form appears naturally in the projection algorithm,[4,7] the rhombs being the projections of the two-faces of the original five-dimensional hypercubic lattice. If one cuts these polygons in a particular way, one obtains two types of *triangles*, P and Q (see Fig. 1), which were first considered by Robinson.[11,12] They will be referred to as A-tiles. The A-tiling is subject to the following two *matching rules*:

1. Each vertex of a triangle carries a color (black or white). Each edge of a triangle must be abutted by the edge of another one in such a way that the colors of the vertices match.

2. In the case of a monochromatic edge (joining two vertices of the same color), the smaller angle of one triangle must abut the smaller angle of the other. This is equivalent to saying that each monochromatic edge is oriented, and the orientations of monochromatic edges of adjacent tiles must match.

Let us now describe the exact *inflation rules* of this tiling. The A-tiles can be composed to form new tiles (see Fig. 1). Composing P and Q gives the triangle $\tau Q'$, which is deduced from Q by expanding by a linear factor τ and reversing the vertex colors. Thus, there are two basic Robinson tilings with triangles, denoted A and B.

The A-tiling is made of a larger triangle P and a smaller triangle Q. In the B-tiling, the triangle P has become the smaller one, while the larger

triangle is $\tau Q'$. Similarly, the composition of P and $\tau Q'$ forms the triangle $\tau P'$. Consequently there is a third tiling, denoted $\tau A'$, consisting of triangles $\tau P'$ and $\tau Q'$, which is isomorphic (similar) to A, since both triangles are expanded by a factor τ, and have their colors reversed. We may proceed further: by composition, the $\tau A'$-tiles lead to $\tau B'$-tiles, which lead to $\tau^2 A$-tiles. Let us summarize the successive steps:

$$
\begin{aligned}
&\text{(a)} \quad P + Q \to \tau Q' && A(P, Q) \to B(\tau Q', P) \\
&\text{(b)} \quad \tau Q' + P \to \tau P' && B(\tau Q', P) \to \tau A'(\tau P', \tau Q') \\
&\text{(c)} \quad \tau P' + \tau Q' \to \tau^2 Q && \tau A'(\tau P', \tau Q') \to \tau B'(\tau^2 Q, \tau P') \\
&\text{(d)} \quad \tau^2 Q + \tau P' \to \tau^2 P && \tau B'(\tau^2 Q, \tau P') \to \tau^2 A(\tau^2 P, \tau^2 Q)
\end{aligned}
\tag{2.1}
$$

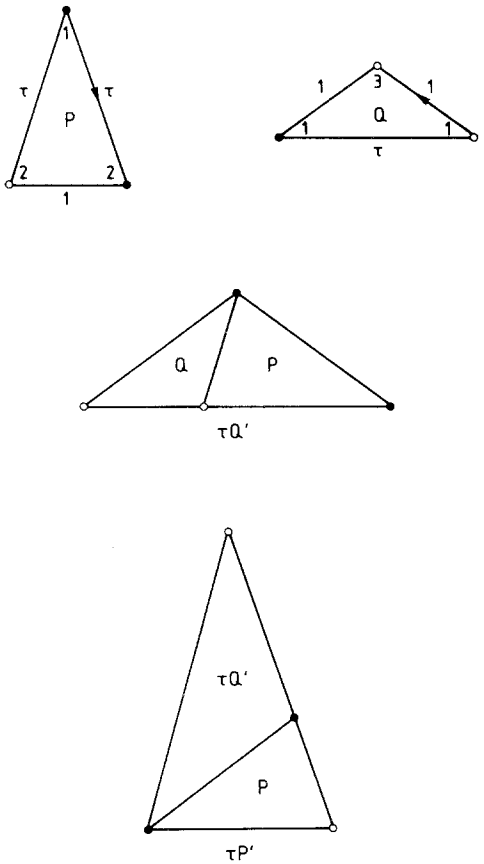

Fig. 1. Robinson triangles and their composition rules. Angles are in units of $\pi/5$; $\tau = (\sqrt{5}+1)/2$ is the golden mean.

In the parentheses the larger tile that appears in the tiling is always written in the first place. The important point for what follows is that, at each step of the composition (deflation) process, the edges and vertices that are deleted are all contained in a particular type of polygon (see Fig. 2). For steps (a) and (c), the compositions take place in a rhomb, while they occur in a kite for steps (b) and (d). Figure 3 shows the different composition steps on a finite sample of the tiling.

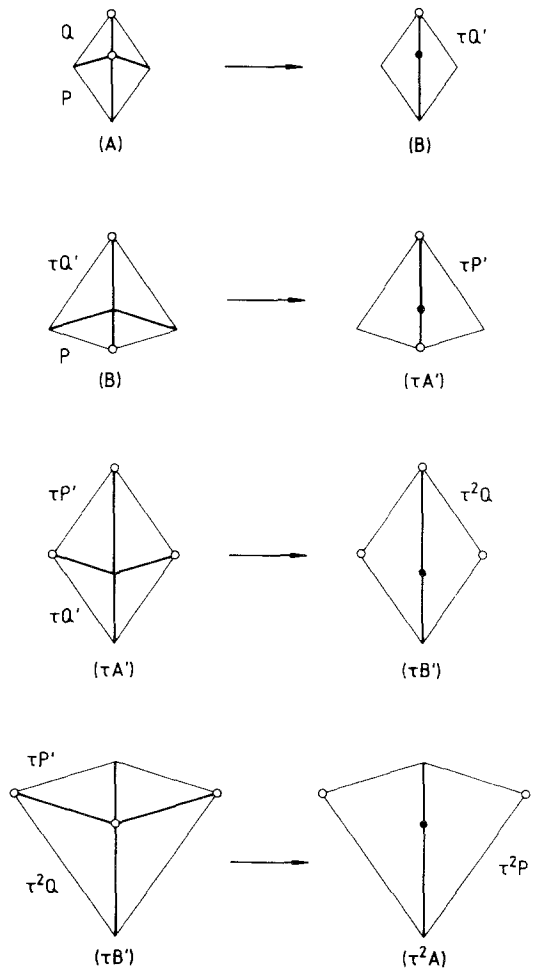

Fig. 2. The four steps of the composition (deflation) procedure [see Eq. (2.1)], showing the rhombs and kites where the elementary compositions take place.

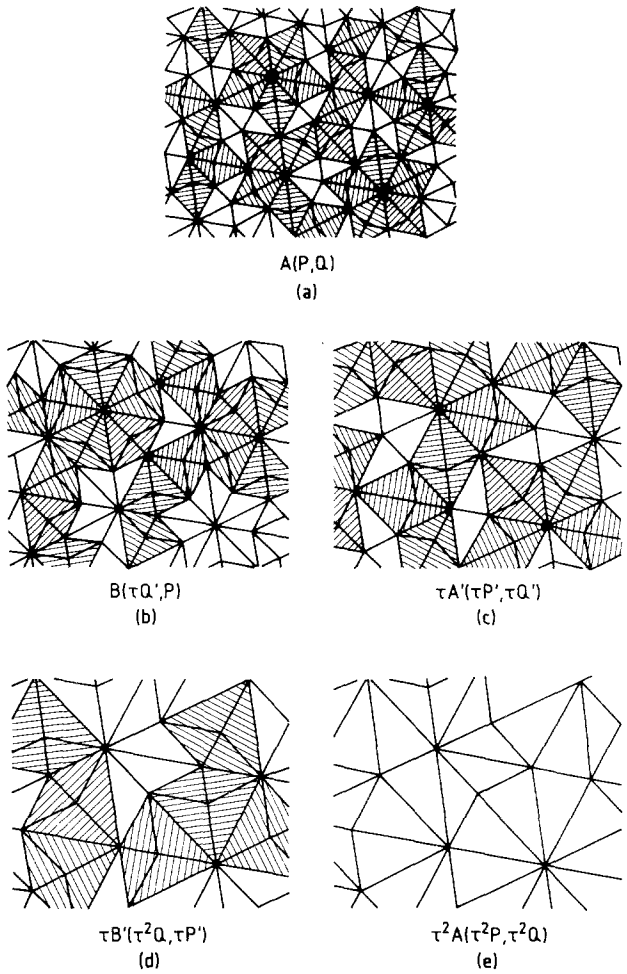

Fig. 3. Finite sample of the Robinson tiling at different steps of the deflation procedure [see Eq. (2.1)]. The shaded areas correspond to the polygons where the next composition step is going to occur. (This figure is a modified version of a figure of Ref. 12.)

2.2. The Ising Model and Its Renormalization

We now define an Ising model on the Robinson tiling and study its properties by means of the Migdal–Kadanoff[13,14] scheme. This real-space renormalization method consists in moving bonds (i.e., edges) of the original lattice in such a way that the spins can be recursively traced out, yielding an approximate solution of the model. It seems natural in the present situation to require that the bond-moving procedure fit the com-

position rules described in Section 2.1. This condition can be consistently fulfilled if the exchange couplings J_{ij} of the Hamiltonian (1.1) are defined in the following *geometrical* way. In the tilings A, B,..., $\tau^2 A$, the lengths of the edges are $1, \tau, \tau^2, \tau^3$. To these sizes we associate the couplings K, L, M, N, respectively. Moreover, we attach to each of these couplings a subscript equal to the number of white vertices at the ends of the corresponding bond. For instance, one finds the couplings K_1, L_1, L_0 around a triangle P, and L_1, K_1, K_2 around a triangle Q. Figure 4 represents the couplings of the three pairs of triangles at different scales $1, \tau, \tau^2$. This shows how the bonds are transformed by composition (deflation)

$$\begin{aligned} K_1 &\to L_1 \to M_1 \\ K_2 &\to L_0 \to M_2 \\ L_0 &\to M_2 \to N_0 \\ L_1 &\to M_1 \to N_1 \end{aligned} \tag{2.2}$$

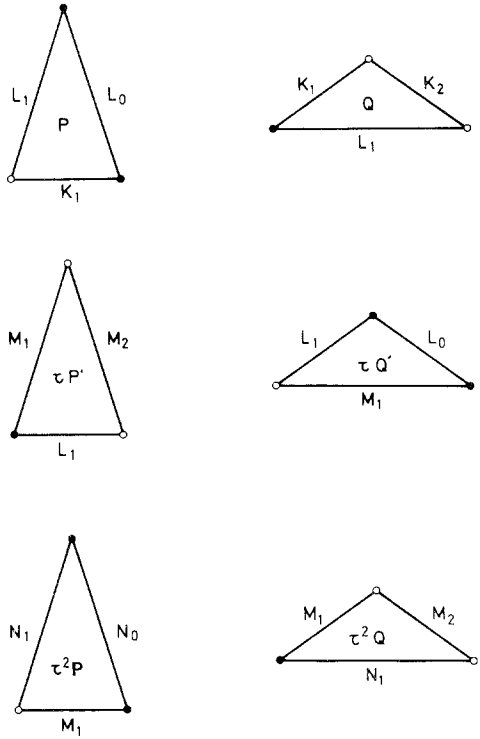

Fig. 4. Geometrical definition of the coupling constants K_1,..., N_1 of our Ising model. Letters and subscripts correspond to bond lengths and numbers of white vertices, respectively (see text).

As was mentioned at the end of last subsection, the composition of triangles always occurs in a certain type of polygon. For each of the four steps of a composition cycle [see Eq. (2.1)], a bond-moving can be attached to the deflation procedure according to the following principle: the bonds that are moved are those that disappear in the composition step under consideration. Let us illustrate this on step (a): $P+Q \to \tau Q'$. Two bonds and one vertex disappear in each rhomb. They both have a coupling K_1. We choose to move one bond K_1 onto K_2, the other one onto L_1. After composition (renormalization), the new bond is M_1. Summing on the initial central spin determines the value of M_1, as well as a contribution A to the free energy; Fig. 5 illustrates the procedure. The central spin σ is coupled to the spin S_L through $K_L = K_1 + K_2$, and to S_R through $K_R = K_1 + L_1$. The unknowns M_1 and A must obey the identity ($S_L, S_R = \pm 1$)

$$A \exp(\beta M_1 S_L S_R) = \sum_{\sigma} \exp[\beta(K_L S_L + K_R S_R)\,\sigma] \tag{2.3}$$

which easily leads to

$$\exp(2\beta M_1) = \frac{\exp(2\beta K_L)\exp(2\beta K_R) + 1}{\exp(2\beta K_L) + \exp(2\beta K_R)} \tag{2.4a}$$

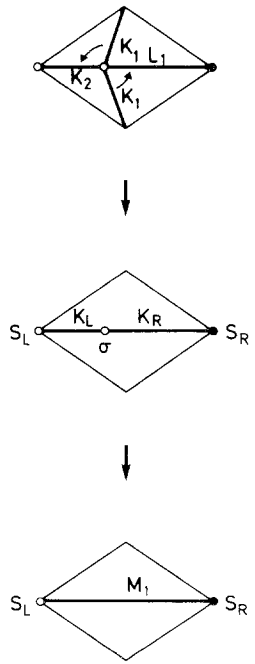

Fig. 5. An elementary bond-moving procedure corresponding to step (a): $P+Q \to \tau Q'$. The renormalized coupling constant M_1 is determined by the identity (2.3).

or equivalently

$$\tanh(\beta M_1) = \tanh(\beta K_L)\tanh(\beta K_R) \tag{2.4b}$$

and

$$A^2 = 4\cosh(\beta K_L + \beta K_R)\cosh(\beta K_L - \beta K_R) \tag{2.4c}$$

The three other steps are dealt with in an analogous way. The full renormalization transformation reads

$$\begin{aligned}
&\text{(a)} \quad \tanh(\beta M_1) = \tanh(\beta K_1 + \beta K_2)\tanh(\beta K_1 + \beta L_1)\\
&\text{(b)} \quad \tanh(\beta M_2) = \tanh(\beta K_1 + \beta L_0)\tanh(\beta L_0 + \beta L_1)\\
&\text{(c)} \quad \tanh(\beta N_1) = \tanh(\beta L_0 + \beta L_1)\tanh(\beta L_1 + \beta M_1)\\
&\text{(d)} \quad \tanh(\beta N_0) = \tanh(\beta L_1 + \beta M_2)\tanh(\beta M_1 + \beta M_2)
\end{aligned} \tag{2.5}$$

This transformation can actually be studied by using only the first two equations, or equivalently by considering only steps (a) and (b), transforming tiling A into $\tau A'$. It can indeed be checked that the full transformation (2.2) is nothing else than the *square* $(\mathcal{T} \circ \mathcal{T})$ of the mapping

$$\mathcal{T}: \quad \begin{aligned} K_1 &\to L_1\\ K_2 &\to L_0\\ L_0 &\to M_2\\ L_1 &\to M_1 \end{aligned} \tag{2.6}$$

describing the renormalization of the A-tiling into the $\tau A'$-tiling.

This property could indeed be expected, since the geometrical transformation $A \to \tau A'$, which amounts to a dilatation of a factor τ and a reversal of the colors of vertices, when squared, leads to the full transformation $A \to \tau^2 A$.

We introduce the following convenient notation of the couplings:

$$J_1 = K_1; \qquad J_2 = K_2; \qquad J_3 = L_0; \qquad J_4 = L_1 \tag{2.7}$$

and the dimensionless variables

$$x_i = \exp(2\beta J_i); \qquad t_i = \tanh(\beta J_i) \tag{2.8}$$

In terms of x_i, the mapping $\mathscr{T}$ we shall use throughout the following assumes a simple *rational* form:

$$\mathscr{T}: \quad \begin{aligned} x_1' &= x_4 \\ x_2' &= x_3 \\ x_3' &= \frac{x_1 x_3^2 x_4 + 1}{x_3(x_1 + x_4)} \\ x_4' &= \frac{x_1^2 x_2 x_4 + 1}{x_1(x_2 + x_4)} \end{aligned} \tag{2.9}$$

while the contributions A and B of steps (a) and (b) to the free energy (see next subsection) are given by

$$\begin{aligned} A^2 &= x_1(x_2 + x_4)[1 + (x_1^2 x_2 x_4)^{-1}] \\ B^2 &= x_3(x_1 + x_4)[1 + (x_1 x_3^2 x_4)^{-1}] \end{aligned} \tag{2.10}$$

The transformation $\mathscr{T}$ has a remarkable property that renormalization maps usually do not have. $\mathscr{T}$ is *invertible*, and its inverse map $\mathscr{T}^{-1}$ is also rational in its four arguments:

$$\mathscr{T}^{-1}: \quad \begin{aligned} x_1 &= \frac{x_1' x_2' x_3' - 1}{x_2'(x_1' x_2' - x_3')} \\ x_2 &= \frac{x_2'(x_1' x_2' - x_3')}{x_1' x_2' x_3' - 1} \frac{x_1' x_4'(x_1' x_2' x_3' - 1) - x_2'(x_1' x_2' - x_3')}{x_1'(x_1' x_2' x_3' - 1) - x_2' x_4'(x_1' x_2' - x_3')} \\ x_3 &= x_2' \\ x_4 &= x_1' \end{aligned} \tag{2.11}$$

This inverse transformation has nevertheless a considerable drawback: the iteration of $\mathscr{T}^{-1}$, starting from *generic* physical values of the x_i, leads to *negative* values of some of these variables, which cannot be interpreted in terms of physical coupling constants.

In terms of the t_i [see Eq. (2.8)], which are nothing else than the *dual* variables of x_i^{-1} [$t_i = (x_i - 1)/(x_i + 1)$], the transformation $\mathscr{T}$ also assumes a simple rational expression:

$$\mathscr{T}: \quad \begin{aligned} t_1' &= t_4 \\ t_2' &= t_3 \\ t_3' &= \frac{t_1 + t_3}{t_1 t_3 + 1} \cdot \frac{t_3 + t_4}{t_3 t_4 + 1} \\ t_4' &= \frac{t_1 + t_2}{t_1 t_2 + 1} \cdot \frac{t_1 + t_4}{t_1 t_4 + 1} \end{aligned} \tag{2.12}$$

2.3. The Free Energy

We now derive an expression for the free energy per site $F(\beta)$ of the model. Consider a very large but finite sample of the Robinson A-tiling having N sites. Since all the facets of the tiling are triangles, it can be easily derived that the sample has $3N$ bonds and $2N$ facets (up to boundary contributions that we shall not consider hereafter, dealing only with thermodynamic quantities). Since the P triangles are τ times more numerous than the Q triangles, their numbers read $N_p = 2\tau^{-1}N$; $N_Q = 2\tau^{-2}N$. In step (a) of the deflation procedure, $P + Q \to \tau Q'$, we trace out $\frac{1}{2}N_Q = \tau^{-2}N$ spins in rhombs. Hence we collect $\tau^{-2}N$ factors A and are left with $N_{Q'} = 2\tau^{-2}N$ and $N_p = 2\tau^{-3}N$ triangles, building the B-tiling. Similarly in step (b), $P + \tau Q' \to \tau P'$, we trace out $\frac{1}{2}N_p = \tau^{-3}N$ spins in kites, we collect $\tau^{-3}N$ factors B, and are left with $N_{p'} = 2\tau^{-3}N$ and $N_{Q'} = 2\tau^{-4}N$ triangles, building the $\tau A'$-tiling. The partition functions Z and Z' of the tilings A and $\tau A'$ are therefore related through

$$Z = A^{\tau^{-2}N} B^{\tau^{-3}N} Z' \tag{2.13}$$

and the free energy F per site obeys the functional equation

$$\beta F(x_i) = \tau^{-2}[\beta F(\mathcal{T}(x_i)) - D(x_i)] \tag{2.14}$$

with

$$D(x_i) = \ln A(x_i) + \tau^{-1} \ln B(x_i) \tag{2.15}$$

By iterating Eq. (2.14), we obtain the following representation of the free energy in terms of all iterates of the renormalization mapping $\mathcal{T}$:

$$\beta F(x_i) = -\sum_{n \geqslant 0} \tau^{-2(n+1)} D[\mathcal{T}^n(x_i)] \tag{2.16}$$

This expression is only a formal solution of the model, since it involves the whole *orbit* $\mathcal{T}^n(x_i)$ by the renormalization transform $\mathcal{T}$ of the initial conditions x_i. We shall see hereafter that this orbit may be very complicated as soon as some *frustration* is present in the model, i.e., if at least one of the exchange couplings J_i is negative. In Section 3 we shall discuss and illustrate several features of the model, both at zero and finite temperature, showing how a "simple" rational map in four variables can lead to extremely intricate outcomes.

2.4. Zero-Temperature Renormalization and Ground-State Energy

The renormalization mapping $\mathscr{T}$ assumes an even simpler (piecewise linear) form $\mathscr{T}_0$ at *zero temperature*, in terms of the couplings J_i. Indeed, the $\beta \to \infty$ limit of Eq. (2.9) reads

$$\mathscr{T}_0: \quad \begin{aligned} J_1' &= J_4 \\ J_2' &= J_3 \\ J_3' &= \tfrac{1}{2}(|J_1 + 2J_3 + J_4| - |J_1 - J_4|) \\ J_4' &= \tfrac{1}{2}(|2J_1 + J_2 + J_4| - |J_2 - J_4|) \end{aligned} \tag{2.17}$$

This expression is easily deduced from Eq. (2.9) by keeping track of the leading powers of e^{β}.

The transformation $\mathscr{T}_0$ is *not* invertible, since the inverse of $\mathscr{T}$ given in Eq. (2.11) does not have a well-defined zero-temperature limit.

An analogous simplification occurs in the expression (2.16) of the free energy. Namely the *ground-state energy* per site $E_0 = \lim_{\beta \to \infty} F(\beta)$ is given by

$$E_0(J_i) = -\sum_{n \geqslant 0} \tau^{-2(n+1)} D_0[\mathscr{T}_0^n(J_i)] \tag{2.18}$$

with

$$D_0(J_i) = \tfrac{1}{2}(|2J_1 + J_2 + J_4| + |J_2 - J_4|) + \tfrac{1}{2}\tau^{-1}(|J_1 + 2J_3 + J_4| + |J_1 - J_4|) \tag{2.19}$$

This expression always leads to a negative value for E_0, as it should, since the internal energy vanishes by definition at infinite temperature.

For *ferromagnetic* models (J_i all positive), it can be checked that Eq. (2.18) leads to

$$-E_0 = J_1 + \tau^{-2} J_2 + \tau^{-1} J_3 + J_4 \tag{2.20}$$

Since all interactions are satisfied at $T = 0$ in these models, Eq. (2.20) means that, among the $3N$ bonds of a sample having N sites, the numbers of bonds of each type discussed in Section 2.2 read asymptotically N, $\tau^{-2}N$, $\tau^{-1}N$, and N, respectively. These frequencies can indeed be derived geometrically, just as we did for the triangles at the beginning of the last subsection. They can also be obtained through the composition rules themselves. Indeed the numbers of bonds N_i ($1 \leqslant i \leqslant 4$) of a finite sample of A-tiling and N_i' of the same sample of $\tau A'$-tiling obtained after steps (a)

and (b) of the deflation procedure are related through the following linear equations:

$$\begin{pmatrix} N_1 \\ N_2 \\ N_3 \\ N_4 \end{pmatrix} = \begin{pmatrix} 0 & 0 & 1 & 2 \\ 0 & 0 & 0 & 1 \\ 0 & 1 & 2 & 0 \\ 1 & 0 & 1 & 1 \end{pmatrix} \begin{pmatrix} N'_1 \\ N'_2 \\ N'_3 \\ N'_4 \end{pmatrix} \tag{2.21}$$

which are a direct consequence of the composition rules (2.1). This matrix has eigenvalues ± 1 and $\tau^{\pm 2}$. The leading eigenvalue is τ^2, as expected, because the inflation rules imply a dilation by a linear factor of τ. The associated eigenvector is $(1; \tau^{-2}; \tau^{-1}; 1)$: its components are proportional to the frequencies we have just described, since the iterates of any initial values of N_i after a large number of inflation steps will be proportional to the components of the leading eigenvector.

3. PHYSICAL PROPERTIES

3.1. The Ferromagnetic Transition

We first consider the case where the exchange couplings J_i are all positive. As expected, we find a single continuous phase transition. More precisely, at high temperature the variables x_i are attracted by the *paramagnetic* (infinite-temperature) fixed point $x_1 = \cdots = x_4 = 1$, while they flow at low temperature toward the *ferromagnetic* (zero-temperature) fixed point $x_1 = \cdots = x_4 = +\infty$. These two regimes are separated by a critical temperature T_c, which smoothly depends on the couplings J_i. The associated variables x_i flow toward the unstable fixed point $x_1 = \cdots = x_4 = x^*$, where $x^* = 1.839287$ is the real solution of $x^3 - x^2 - x - 1 = 0$. This unique, nontrivial fixed point has a remarkable property: it is "isotropic," i.e., all the variables x_i are equal. Hence, it coincides with the fixed point of the usual Migdal–Kadanoff transformation on a triangular (or square) lattice:

$$\mathscr{T}_{\text{reg}}: \quad x \to \frac{x^4 + 1}{2x^2} \tag{3.1}$$

since this mapping is identical to the last two lines of ours [see Eq. (2.9)] if all the x_i are given a common value x.

For "isotropic" models ($J_i = 1$) on triangular and square lattices, the exact values of β_c read

$$\begin{aligned} \beta_c(\triangle) &= \tfrac{1}{4} \ln 3 = 0.274653 \\ \beta_c(\square) &= \tfrac{1}{2} \ln(\sqrt{2} + 1) = 0.440687 \end{aligned} \tag{3.2a}$$

while the Migdal–Kadanoff scheme [Eq. (3.1)] leads to *the same* prediction in both cases

$$\beta_c(\mathrm{MK}) = \tfrac{1}{2} \ln x^* = 0.304689 \tag{3.2b}$$

We therefore find it hard to believe too seriously the prediction of our approach for the critical point of the model $J_i = 1$, which is also given by Eq. (3.2b). Some preliminary Monte Carlo results concerning the ferromagnetic Ising model on a slightly different Penrose tiling suggest, however, that the critical temperature should not be very different from that of a triangular lattice.

The linearization of the mapping $\mathscr{T}$ around its fixed point $x_i = x^*$ allows one to compute the thermal critical exponent ν through

$$\nu = \ln \tau / \ln \mu \tag{3.3}$$

where τ is the dilatation ratio of our renormalization scheme, while μ is the largest eigenvalue of the Jacobian matrix $\mathscr{J}$ ($\mathscr{J}_{ij} = \partial x_i'/\partial x_j$) evaluated at $x_i = x^*$. We find $\mu = 1.401482$, and hence $\nu = 1.425686$. It is clear that this numerical value cannot either be taken too seriously. Let us recall that the usual Migdal–Kadanoff procedure [Eq. (3.1)] for regular lattices (dilatation factor $b = 2$) leads to a value $\nu = 1.338262$. We are led by physical reasons to expect that the critical behavior of the usual Ising model, and in particular the value $\nu = 1$, is *not* modified by the lack of periodicity of Penrose tilings (see introduction). It will be clear in the following that the ferromagnetic transition is by far not the most interesting outcome of our approach.

The singular part of the free energy (2.16) around the critical temperature has the form

$$F_{\mathrm{sg}} \sim |T - T_c|^{2\nu} \tag{3.4a}$$

(since the exponent α equals $2 - 2\nu$). Hence the specific heat

$$C = -\beta^2 \partial^2 (\beta F)/\partial \beta^2 \tag{3.4b}$$

is continuous, but has an infinite slope, at T_c. Figure 6 shows a plot of C against temperature for the "isotropic" model with $J_i = 1$. This curve will be compared in the following with analogous plots for frustrated models.

3.2. Zero-Temperature Phase Diagram

We have seen that the renormalization transformation assumes a simple piecewise linear form $\mathscr{T}_0$ [see Eq. (2.17)] at zero temperature. This

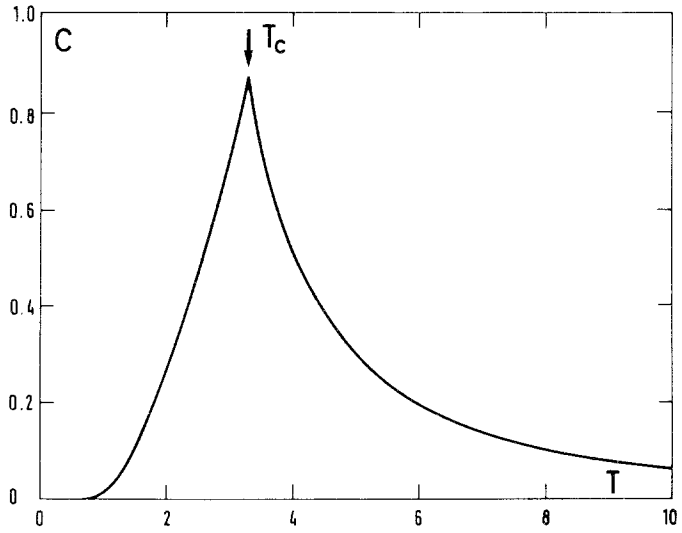

Fig. 6. Plot of the specific heat of the "isotropic" ferromagnetic model against temperature. The critical singularity at $T_c = 3.2820$ is very clearly visible.

apparently simple transform nevertheless leads to a very rich and intricate behavior. A model is given by its four coupling constants J_i, i.e., by a representative point in the four-dimensional J-space. The zero-temperature properties do not depend on the global scale of the J_i: in particular, the mapping $\mathcal{T}_0$ is a *homogeneous* function, as it should be.

The space of all possible models can be divided into *two regions*, according to their zero-temperature properties, in close connection with the asymptotic behavior of the orbit $\mathcal{T}_0^n(J_i)$ at large n.

I. *Quasiferromagnetic region.* If the iterates $\mathcal{T}_0^n(J_i)$ diverge to infinity as the generation label n gets large, then the model presents *long-range order* at zero temperature, which persists as long as temperature is lower than some *finite* critical value $T_c(J_i)$. The prototypes of this class of models are the ferromagnetic ones, for which the action of $\mathcal{T}_0$ reads (except maybe at the very first steps)

$$\begin{pmatrix} J_1' \\ J_2' \\ J_3' \\ J_4' \end{pmatrix} = \begin{pmatrix} 0 & 0 & 0 & 1 \\ 0 & 0 & 1 & 0 \\ 1 & 0 & 1 & 0 \\ 1 & 1 & 0 & 0 \end{pmatrix} \begin{pmatrix} J_1 \\ J_2 \\ J_3 \\ J_4 \end{pmatrix} \tag{3.5}$$

The four couplings $\mathcal{T}_0^n(J_i)$ therefore diverge as λ^n, where $\lambda = 1.512876$ is the leading eigenvalue of the matrix appearing in Eq. (3.5). Usual renor-

malization schemes for models on regular lattices satisfy $\lambda = b^{D-1}$ (where b is the dilatation scale and D the dimension). We interpret the fact that λ is (slightly) different from τ in the present case as being a (harmless) pathology of our approximate solution.

More generally, since each model of the ordered region falls after a *finite* number n_0 of renormalization steps onto the limit map (3.5), the long-range order it exhibits is characterized by a modulation of the order parameter up to a maximal scale τ^{n_0}. This type of order, which generalizes to aperiodic systems the antiferromagnetic order, or the modulated order encountered, e.g., in ANNNI models, can be named *quasiferromagnetism.* This phenomenon is already present in the 1D Ising model in a quasicrystalline magnetic field.[15]

II. "*Disordered*" *region.* This region is defined as being the complement of the previous one, i.e., the set of models such that the orbit of couplings $\mathscr{T}_0^n(J_i)$ does not go to infinity. This negative definition embraces quite a variety of different behaviors. This region is nevertheless essentially made up of *two* types of models:

IIa. Models such that $\mathscr{T}_0^n(J_i)$ vanish identically for n larger than some n_0.

IIb. Models such that $\mathscr{T}_0^n(J_i)$ lie exactly on a two-cycle of the form

$$(a; 0; 0; 0) \leftrightarrow (0; 0; 0; a) \tag{3.6}$$

for n larger than some n_0. The positive number a varies continuously with the couplings J_i inside region IIb.

We have determined the relative weights of regions I, IIa, and IIb as follows. Since the transformation $\mathscr{T}_0$ is homogeneous in the four variables J_i, the regions we have defined are *cones* extending to infinity in the J-space. A convenient way of dividing out this infinity is to restrict oneself to models such that $\sum_{i=1}^{4} J_i^2 = 1$, i.e., to look at the unit *sphere* S_3 of the J-space. The weights of the different regions are now well-defined as being the measure of their intersection with S_3 (the measure being the usual isotropic one). By sampling S_3 with a large number of random, isotropically distributed values of J_i, we have obtained rather accurate numerical values of the measure of the different regions of the phase diagram:

$$\text{I: } 92.6\% \qquad \text{II: } 7.4\% \quad (\text{IIa: } 2.6\%; \text{IIb: } 4.8\%) \tag{3.7}$$

The models that lead to a more complicated orbit than the simple kinds of behavior I, IIa, or IIb therefore seem to build a set of zero

measure that can be viewed as the boundaries separating those three regions.

The models of types IIa and IIb, which form the bulk of the "disordered" region, become paramagnetic at any small but nonzero temperature. They *may* nevertheless exhibit some "exotic" kind of long-range order at zero temperature, e.g., a spin modulation which is *incommensurate* with the Penrose tiling, or a *topological* X–Y type order, etc. These cases (if any), which do not belong to our definition of quasiferromagnetic order, are more subtle phenomena that our bond-moving procedure cannot describe accurately. The name "disordered" that we have attached to region II for simplicity therefore fully deserves its quotation marks. Moreover, models of regions IIa and IIb may develop quasiferromagnetic long-range order at higher temperature through a reentrant phenomenon to be discussed later.

Let us illustrate how intricate the division of the J-space into regions I and II can be, by showing a few sections (this is indeed the best one can

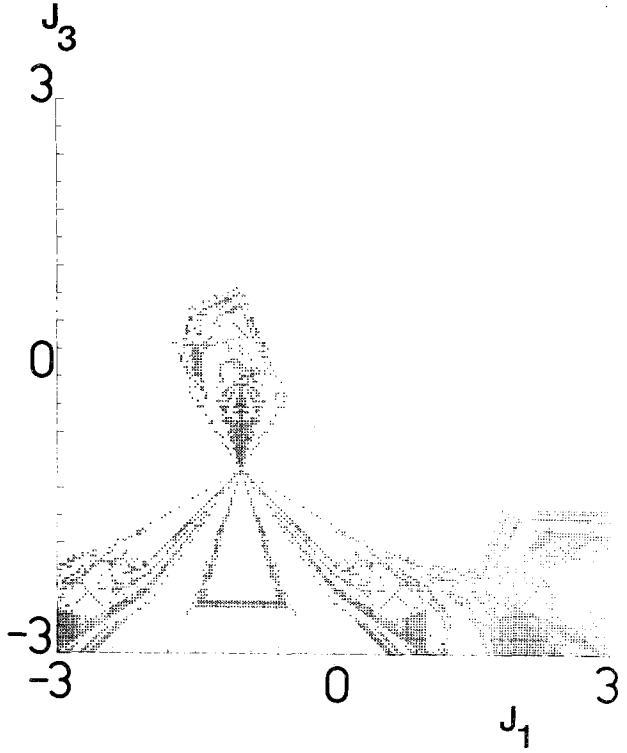

Fig. 7. Zero-temperature phase diagram in the (J_1, J_3) plane (J_2 and J_4 are kept equal to $+1$). White and dark areas correspond to regions I and II, respectively (see text).

hope to do when dealing with a four-dimensional space). In each of these plots, two couplings are kept fixed, equal to $+1$, while the two others are varied and used as coordinates. White areas correspond to region I (quasiferromagnetic models); dark areas to region II. Figures 7 and 8 show the (J_1, J_3) and (J_2, J_4) planes, respectively. Figure 9 is a rather esthetic enlargement of Fig. 7. We may have missed much more appealing details of the division of J-space according to zero-temperature behavior; we hope nevertheless to have shown convincingly that the phase diagram we get is fairly complicated.

3.3. Finite-Temperature Phase Diagram

In this subsection we aim to capture some features of the frustrated models at finite temperature. We have seen that most models (region I) exhibit quasiferromagnetic order at $T=0$, while some do not (region II). These two regions interpenetrate in a very intricate fashion. We shall now

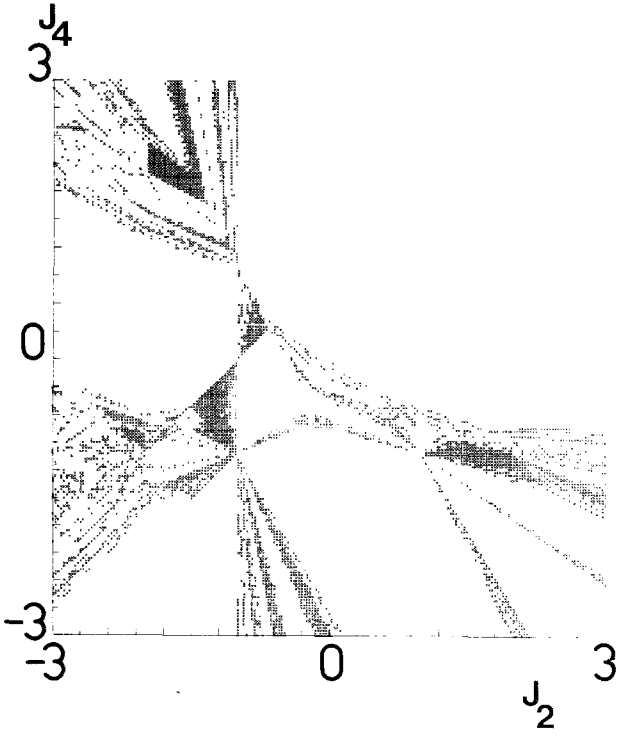

Fig. 8. Same as Fig. 7, in the (J_2, J_4) plane (J_1 and J_3 are kept equal to $+1$).

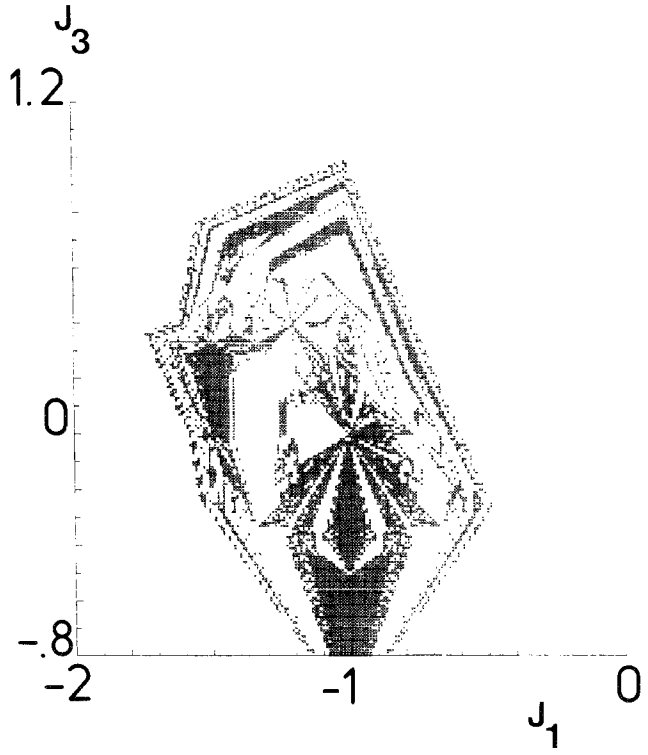

Fig. 9. Enlargement of the central part of Fig. 7.

describe how this zero-temperature picture is modified when thermal fluctuations are taken into account.

In analogy with the zero-temperature properties discussed in the last subsection, we have explored the five-dimensional (J, T) space along some sections. Figures 10 and 11 show plots of the phase diagram when *one* combination of the couplings J_i and temperature are simultaneously varied: the abscissa reads $J = J_3 = J_4$ (with $J_1 = J_2 = +1$) for Fig. 10; $J = J_1 = J_3$ (with $J_2 = J_4 = +1$) for Fig. 11; the ordinate is just T. White areas correspond to disordered phases with *paramagnetic* behavior (variables x_i attracted by the infinite-temperature fixed point), while dark areas correspond to long-range quasiferromagnetic order [i.e., $\mathcal{T}^n(x_i) \to +\infty$]. The boundaries between both kinds of domains are just sections of the critical surface $T_c(J_i)$. The essential new feature that shows up is the existence of *reentrant* phases. A given model may undergo *several* phase transitions when temperature is increased. In particular, there are models in region II that have no order as $T \to 0$, but become ordered between two finite critical tem-

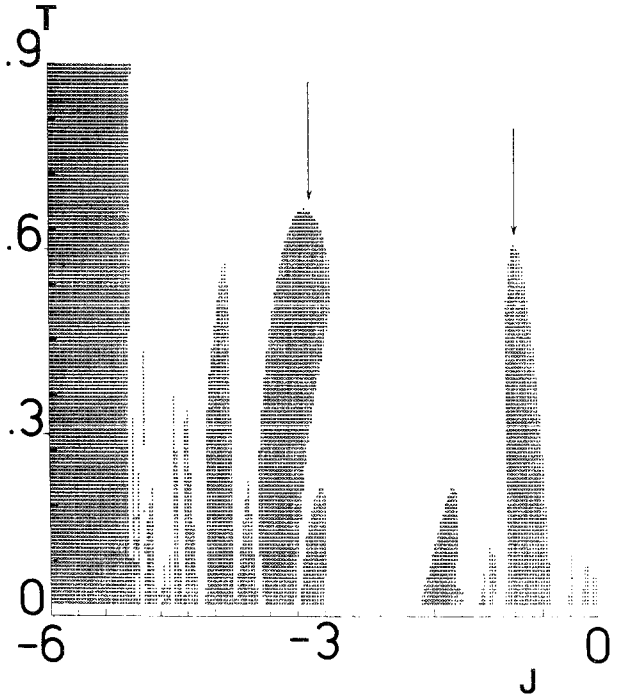

Fig. 10. Finite-temperature phase diagram along the section $J_1 = J_2 = +1$; $J_3 = J_4 = J < 0$, in the (J, T) plane. Dark areas correspond to ordered (quasiferromagnetic) phases. Arrows indicate the models for which specific heat plots are presented in Figs. 12–14.

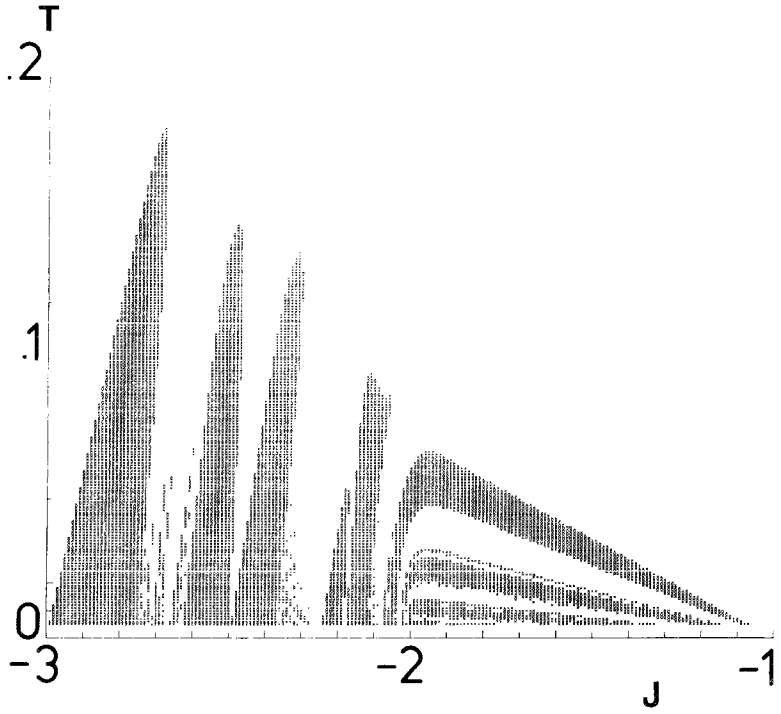

Fig. 11. Same as Fig. 10, along the section $J_2 = J_4 = +1$; $J_1 = J_3 = J < 0$. A series of at least three successive reentrant phases can be seen on the right half of the figure.

peratures. More generally, the critical surface exhibits a complicated multivalued structure, allowing a large variety of sequences of ordered (quasiferromagnetic) and disordered (paramagnetic) phases. Around the values of T_c that demarcate all these phases, the model exhibits qualitatively *the same* critical behavior as in the ferromagnetic region, since the associated variables x_i always flow toward the fixed point $x_i = x^*$ described in Section 3.1 (this is indeed the unique nontrivial real fixed point of the mapping $\mathcal{T}$). The critical singularities of the free energy are nevertheless generically much less pronounced than in the ferromagnetic case.

Let us illustrate the thermal effects of reentrance phenomena present in our model by specific heat plots of two typical cases. These plots are to be compared with Fig. 6 corresponding to the isotropic ferromagnetic case. Figure 12 shows a generic frustrated model ($J_1 = J_2 = +1$; $J_3 = J_4 = -0.9$) that does *not* exhibit reentrant behavior. Rather strikingly, the critical singularity is very hardly visible at the scale of the plot, which shows above all a large but smooth maximum at $T^* \approx 2.5 T_c$. Hence, the most important rearrangements that occur in the system when temperature is increased are not closely related to the disappearance of long-range order, but take place at a different energy scale T^*. Figures 13 and 14 correspond to a model ($J_1 = J_2 = +1$; $J_3 = J_4 = -3.2$) that exhibits two ordered phases (a normal one at low temperature, and a reentrant one) and hence three critical tem-

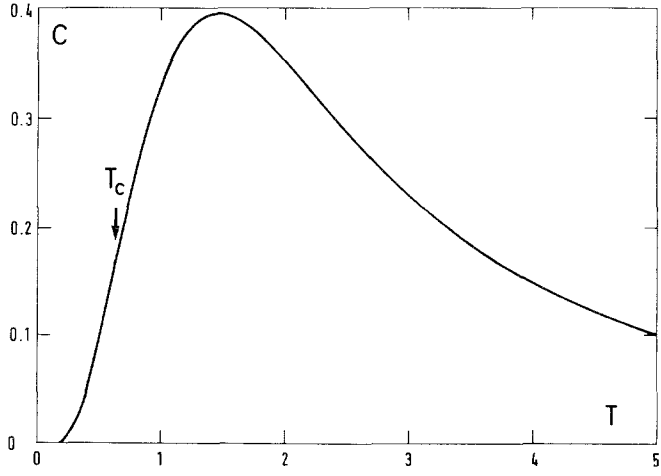

Fig. 12. Plot of the specific heat of a frustrated model ($J_1 = J_2 = +1$; $J_3 = J_4 = -0.9$) without reentrant behavior. The critical singularity ($T_c = 0.60592$) is hardly visible.

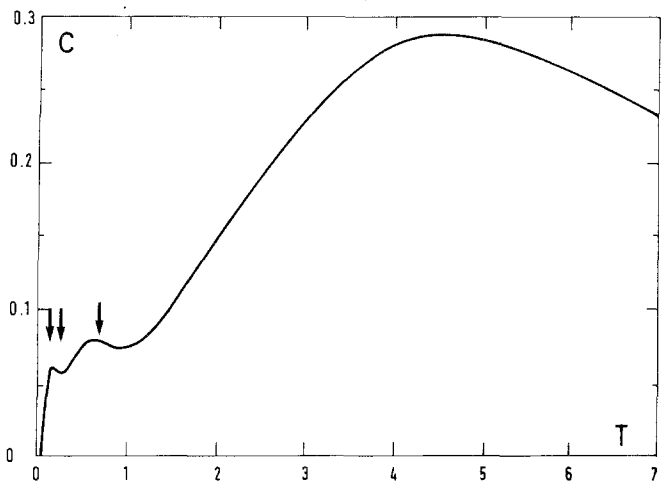

Fig. 13. Plot of the specific heat of a frustrated model ($J_1 = J_2 = +1$; $J_3 = J_4 = -3.2$) with two ordered phases: a normal one ($0 < T < T_c^{(1)}$) and a reentrant one ($T_c^{(2)} < T < T_c^{(3)}$).

peratures. Figure 13 shows a global picture of the variations of the specific heat; Fig. 14 is an enlargement at low temperature, showing that the reentrance phenomenon leads to a smooth but nonmonotonic temperature dependence. The three critical singularities are not visible at that scale. The temperature T^* where the specific heat is maximal is roughly one order of magnitude above the critical temperature!

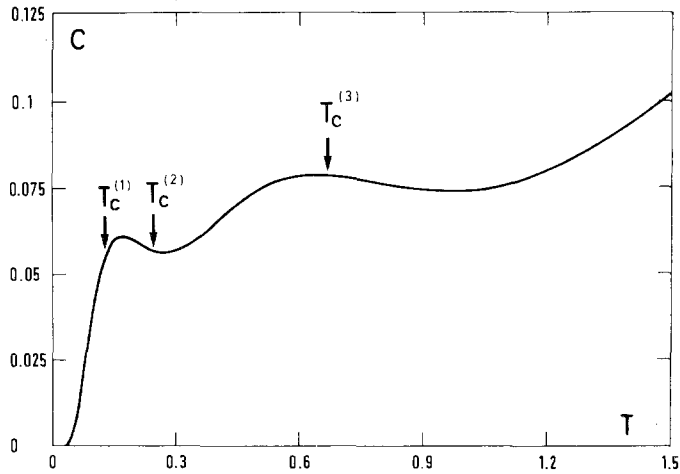

Fig. 14. Enlargement of the low-temperature region of Fig. 13, showing the structure of $C(T)$ around the critical temperatures $T_c^{(1)} = 0.13121$, $T_c^{(2)} = 0.24644$, $T_c^{(3)} = 0.66320$.

4. CONCLUSION

Through the present study, the Migdal–Kadanoff renormalization scheme has proven to be a natural method to use in order to study the magnetic phase structure on the Penrose lattice, since it follows exactly the geometry of the system. Though it has approximate character, this method is expected to reflect properties of the Ising model on a real 2D quasiperiodic lattice, at least concerning its qualitative behavior.

The most interesting aspect of the present study is certainly the richness of the phase diagram of this Ising model. In particular, the case where the couplings have both signs is an interesting example of frustration without randomness. The situation is indeed very different from the one on a periodic lattice: because of aperiodicity, the unit cell of the quasicrystal has an infinity of atoms, and each spin experiences a different environment.

For most values of its four coupling constants (region I), the model exhibits a long-range "quasiferromagnetic" order, characterized by a modulation that has the same type of quasiperiodicity as the underlying lattice. This order persists up to some finite temperature T_c and may also appear again at higher temperature through a reentrant mechanism. This situation reminds one of the cases of commensurate modulation met, e.g., in ANNNI models. Other types of order (incommensurate, topological, etc.), which cannot be attained by our approach, could possibly exist at zero temperature in the "disordered" models, for which T_c vanishes (region II).

We finally mention that the mere description of the exact ground state(s) of the frustrated Ising model on a quasiperiodic tiling remains an open difficult question, related to problems found in optimization. Indeed, the system exhibits a high level of complexity.

ACKNOWLEDGMENT

C. G. thanks J. F. Sadoc for having made him aware of the unpublished work of R. Robinson.

REFERENCES

1. D. Schechtman, I. Blech, D. Gratias, and J. W. Cahn, *Phys. Rev. Lett.* **53**:1951 (1984).
2. Workshop on Aperiodic Crystals, Les Houches (March 1986), *J. Phys. Colloques (Paris)* **C3** (1986).
3. R. Penrose, *Math. Intell.* **2**:32 (1979); M. Gardner, *Sci. Am.* **236**:110 (1977).
4. N. G. de Bruijn, *Ned. Akad. Wet. Proc. A* **43**:39 (1981).
5. M. Duneau and A. Katz, *Phys. Rev. Lett.* **54**:2688 (1985).
6. V. Elser, *Phys. Rev. B* **32**:4892 (1985).

7. P. A. Kalugin, A. Yu. Kitayev, and L. S. Levitov, *J. Phys. Lett. (Paris)* **46**:L601 (1985); *JETP Lett.* **41**:145 (1985).
8. G. Toulouse, *Commun. Phys.* **2**:115 (1977).
9. S. R. McKay, N. Berker, and S. Kirkpatrick, *Phys. Rev. Lett.* **48**:767 (1982), and references therein.
10. B. Derrida, J. P. Eckmann, and A. Erzan, *J. Phys. A* **16**:893 (1983).
11. R. Robinson, University of California preprint (1975), unpublished.
12. B. Grünbaum and G. C. Shepard, *Tilings and Patterns*, Freeman, New York, Chapter 10.
13. A. A. Migdal, *Sov. Phys. JETP* **42**:743 (1975).
14. L. P. Kadanoff, *Ann. Phys. (N.Y.)* **100**:359 (1976).
15. J. M. Luck, *J. Phys. A*, to be published.
16. J. M. Luck and Th. M. Nieuwenhuizen, *Europhys. Lett.* **2**:257 (1986).
17. Y. Achiam, T. C. Lubensky, and E. W. Marshall, *Phys. Rev.* **33**:6460 (1986).
18. C. Godrèche and H. Orland, in Ref. 2.
19. Th. Niemeijer and J. M. J. van Leeuwen, in *Phase Transitions and Critical Phenomena*, Vol. 6, C. Domb and M. S. Green, eds. (1976).